# Ultrafast Laser-induced Structural Changes in Semiconductors

E. Mazur, E.N. Glezer, L. Huang, and J.P. Callan
Harvard University, Gordon McKay Laboratory
9 Oxford Street, Cambridge, MA 02138, USA

## ABSTRACT

We present experimentally determined values of the dielectric function of GaAs following femtosecond laser excitation. The data at photon energies of 2.2 and 4.4 eV show that the response of the dielectric function to the excitation is dominated by changes in the electronic band structure and not by the optical susceptibility of the excited free carriers. The behavior of the dielectric function indicates a drop in the average bonding-antibonding splitting of GaAs following the excitation, which leads to a collapse of the band gap. The changes in the electronic band structure result from a combination of electronic screening, many-body effects, and structural deformation of the lattice caused by the destabilization of the covalent bonds. Broadband measurement of the dielectric function over the range 1.5–3.5 eV reveals ultrafast laser-induced heating at low fluence, disordering at intermediate fluence, and an ultrafast semiconductor-to-metal transition at high fluence.

**Keywords:** GaAs, laser-induced phase transition, dielectric function, ultrafast

## 1. INTRODUCTION

The field of laser-induced phase transitions in semiconductors dates back to the discovery in the 1970's that semiconductor crystals can be 'annealed' by irradiation with a short intense laser pulse[1]. Following the first experiments, two models were proposed to explain the structural change resulting from the laser excitation. One model, known as the thermal model, describes the structural change as a thermal melting process.[2–4] The thermal model assumes that the hot electrons rapidly equilibrate with the lattice by exciting lattice vibrations through phonon emission. With this assumption, the laser energy deposited in the material can be treated as though it is instantly converted to heat. If the incident laser pulse is strong enough, the irradiated part of the sample will heat up to the melting temperature and undergo a transition to the liquid phase as the latent heat of fusion is supplied.

The other model, known as the plasma model, attributes the structural change to destabilization of the covalent bonds resulting directly from the electronic excitation.[5,6] The plasma model assumes a slow rate of phonon emission by the excited electronic system compared to the energy deposition time (*i.e.*, the laser pulse width). According to this model, the structural change is driven directly by the excited electronic system. If a high enough fraction of the valence electrons is excited from bonding states to antibonding states, the crystal becomes unstable, and a structural phase transition occurs.

With nanosecond and picosecond pulses the transition from solid to liquid is thermal: because of the fast coupling between carriers and phonons, the electrons and the lattice are in thermal equilibrium and the material simply melts. A detailed account of these thermal transitions, including the heating of the solid, thermal diffusion, melting, motion of the interface boundary and recrystallization can be found in Ref. [7]. Here, we concentrate on the highly nonequilibrium dynamics in a semiconductor excited by intense femtosecond pulses.

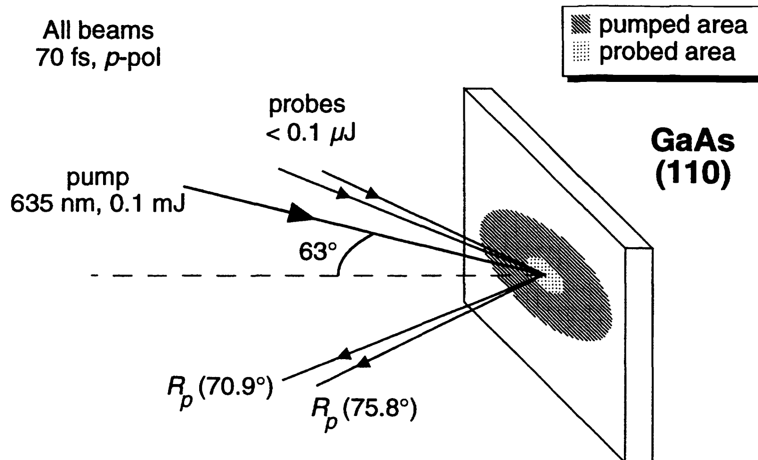


**Figure 1.** Two-angle probe geometry for determining the dielectric constant of GaAs.

Reflectivity and second-harmonic generation studies of femtosecond laser-excited semiconductors show evidence of rapid changes in the material (within a few hundred femtoseconds) following the excitation.[8–13] However, interpretation of reflectivity and second-harmonic generation results is difficult because these quantities do not directly yield the behavior of intrinsic material properties. In particular, the reflectivity at a specific wavelength, polarization, and incident angle depends on both the real and imaginary parts of the dielectric constant at that wavelength. Furthermore, the measured second-harmonic radiation depends on the dielectric constant at both the fundamental and second-harmonic wavelengths as well as on the second-order susceptibility.

In the absence of a direct determination of the dielectric constant, interpretation of reflectivity and second-harmonic data requires making assumptions about the functional form of the dielectric constant, for instance that changes in the dielectric constant induced by the excitation are dominated by the free carrier contribution to the optical susceptibility.[13,14,24] Under this assumption, the changes in the dielectric constant are described by the Drude-model. While this works well at lower excitation regimes, we will show that it leads to incorrect conclusions in the case of laser-induced disordering experiments.

## 2. DIRECT MEASUREMENT OF THE DIELECTRIC CONSTANT AT 2.2 eV

We directly determined the time-evolution of the real and imaginary parts of the dielectric constant using the two-angle probe technique shown in Fig. 1.[28,29] A 70-fs laser pulse at a photon energy of 1.9 eV is used to excite a 0.01-$mm^2$ area on the GaAs surface. The evolution of the reflectivity of the central 6% of the pumped area is measured at two different angles of incidence using 70-fs pulses at a photon energy of 2.2 eV. The probe beam fluence never exceeds 0.1 $kJ/m^2$ so as not to produce any detectable changes in the dielectric constant. To avoid cumulative damage effects, we translate the sample during data collection so that each data point is obtained at a new spot on the sample.

Each pair of reflectivity measurements is converted to a corresponding real and imaginary part of the dielectric constant by numerically inverting the Fresnel formula for reflectivity as a function of incident angle. Setting one of the probe beam angles of incidence to the Brewster angle provides good sensitivity in distinguishing changes in $\mathrm{Re}(\varepsilon)$ from changes in $\mathrm{Im}(\varepsilon)$ because the $p$-polarized reflectivity at this angle is determined mainly by $\mathrm{Im}(\varepsilon)$.[15]

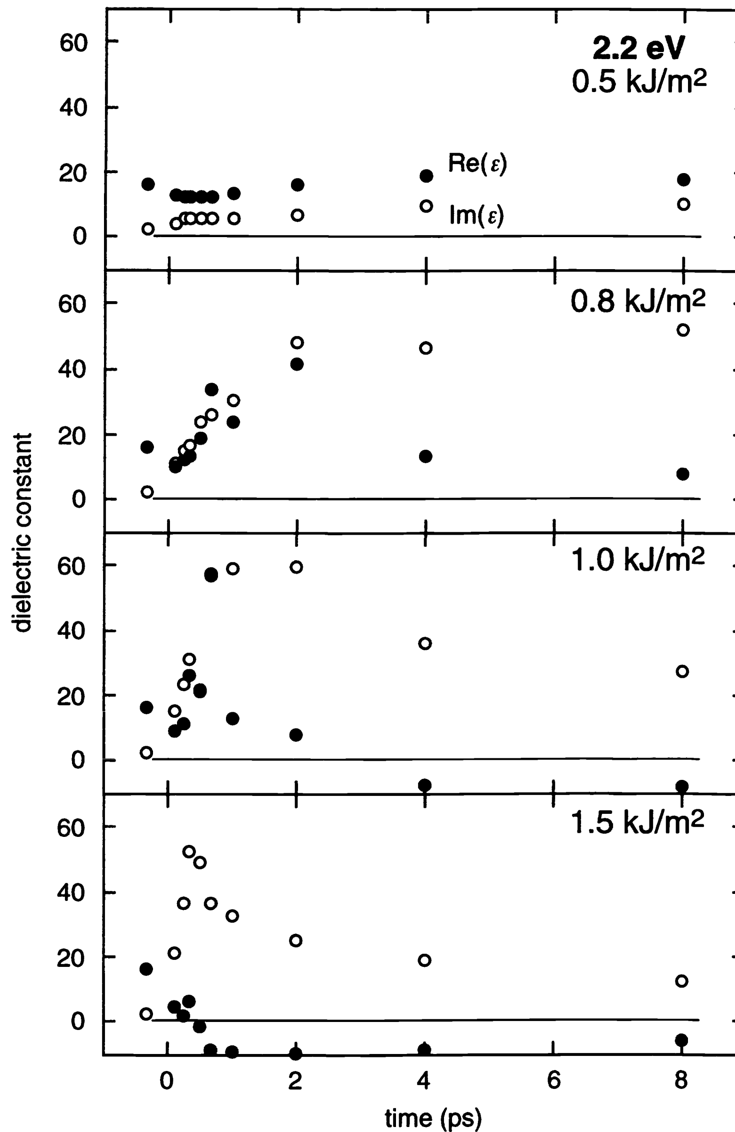


**Figure 2.** Dielectric constant at 2.2 eV vs. pump-probe time delay for four different pump fluences. ●: Re($\varepsilon$), ○: Im ($\varepsilon$).

Figures 2 and 3 summarize the experimental values obtained for the dielectric function at 2.2 eV. In Fig. 2, Re($\varepsilon$) (filled circles) and Im($\varepsilon$) (open circles) are plotted vs. pump-probe time delay for four different excitation fluences; in Fig. 3, Re($\varepsilon$) and Im($\varepsilon$) are plotted vs. pump fluence at four different time delays. The change induced in the dielectric constant by the pump pulse excitation is completely different from that expected from the free carrier contribution to the optical susceptibility. In Fig. 2, at pump fluences near 1 kJ/m$^2$ for instance, Im($\varepsilon$) starts at an initial value of about 2, rises to a peak near 60, and then drops to somewhere between 10 and 15, in strong contrast to the slight, featureless increase predicted by the Drude model. Meanwhile, Re($\varepsilon$) first decreases slightly but then sharply increases before dropping through zero. Note that the zero-crossing of Re($\varepsilon$) roughly coincides with the peak in Im($\varepsilon$).

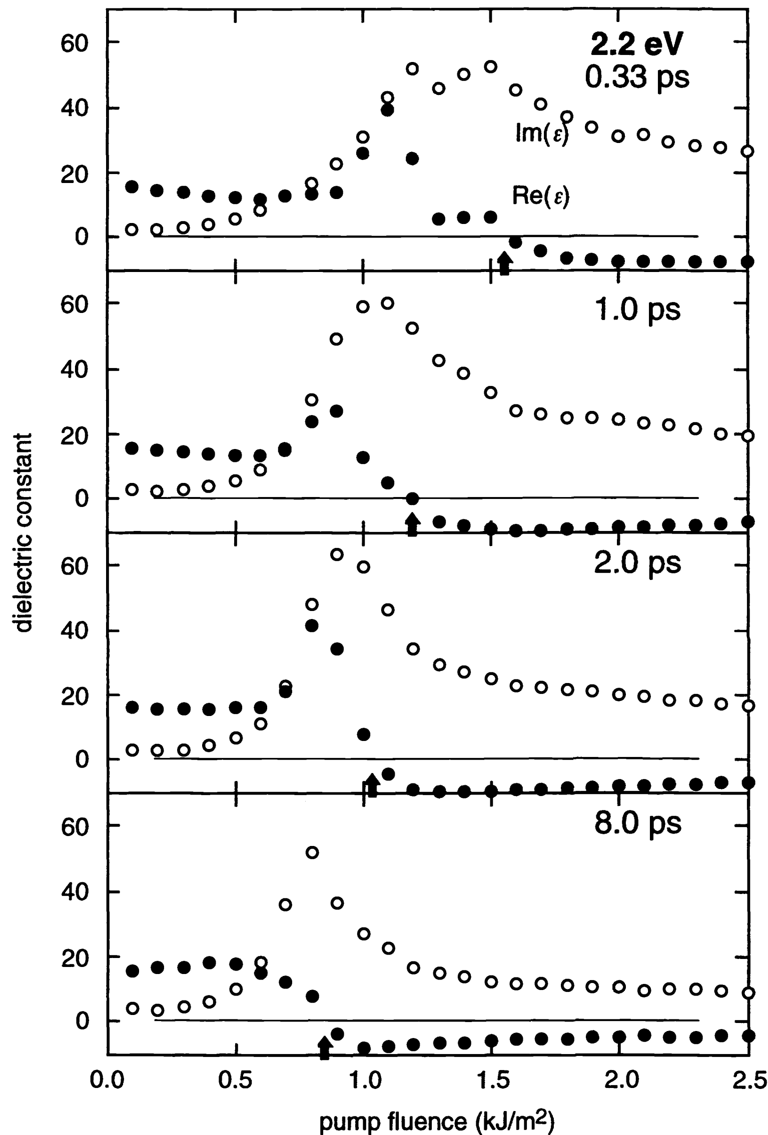


**Figure 3.** Dielectric constant at 2.2 eV vs. pump fluence for four different pump-probe time delays. ●: Re($\varepsilon$), ○: Im ($\varepsilon$).

Figure 4 shows how misleading a single-angle reflectivity measurement can be. The top graph in Fig. *4a* shows experimental values for the *p*-polarized reflectivity at a (single) incident angle of 45°, 2 ps after excitation with a 2.2-eV pump pulse. The bottom graph in Fig. *4a* shows a Drude-like dielectric constant, adjusted to reproduce the measured 45°-reflectivity values as shown by the curve through the reflectivity data in the top graph in Fig. *4a*. The excellent quality of the fit might lead one to conclude that the behavior of the dielectric constant is completely described by the Drude model. The measured dielectric constant, however, behaves very differently as can be seen in the bottom graph in Fig. *4b*, which shows the experimentally determined dielectric constant at 2.2 eV plotted against pump fluence at a time delay of 2 ps (corresponding to the third graph in Fig. 3).. If we use the experimentally determined dielectric constant values from this graph to calculate

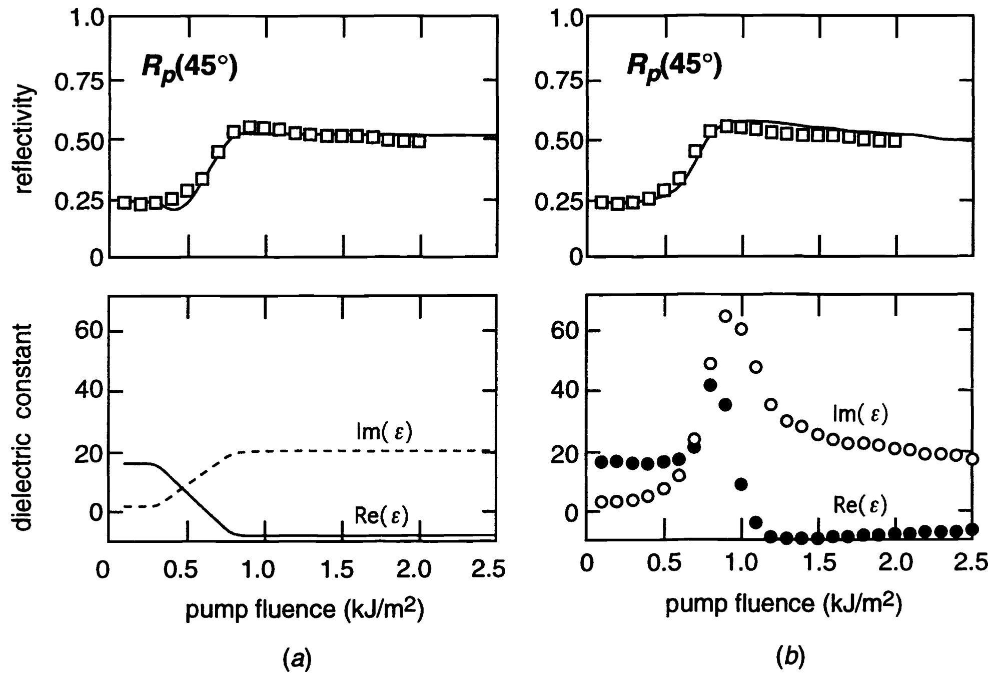


**Figure 4.** Comparison of (*a*) Drude-like dielectric function fitted to single-angle measurement of the reflectivity with (*b*) measured dielectric function. The top graphs show the *p*-polarized reflectivity at 45° incident angle. ——: reflectivity calculated from dielectric constant, □: measured reflectivity.

the corresponding *p*-polarized reflectivity at an incident angle of 45°, we obtain the curve through the data points in the top graph in Fig. 4*b* in excellent agreement with the experimental values. Note, however, how much the actual dielectric constant differs from that following from an assumed Drude-like behavior (bottom two graphs). Only the dielectric constant in Fig. 4*b* correctly accounts for the reflectivities at 45°, 70.9° and 75.8°; the Drude-like dielectric constant only correctly describes the 45° data. Notice, in particular, how the Drude assumption completely misses the strong absorption-like feature in the dielectric function which occurs at 1.0 $kJ/m^2$, precisely as the material undergoes a transition (see also Fig. 5).

The results shown in Figs. 2 and 3 indicate that a strong absorption peak comes into resonance with the probe frequency as a result of the excitation. The resonance behavior is most striking in Fig. 3 because the features are particularly clear when plotted versus pump fluence. This behavior must result from an interband absorption peak and not from a free carrier plasma resonance because the zero-crossing in Re($\varepsilon$) is accompanied by a peak in Im($\varepsilon$) rather than by a steady increase. From the behavior of Re($\varepsilon$), we can infer the time evolution of this interband absorption peak. Because Re($\varepsilon$) is initially positive, the resonant frequency of the observed absorption peak evidently starts out higher than the probe frequency; it then sweeps down through the probe frequency as Re($\varepsilon$) drops through zero.

The rate at which the resonant frequency of the absorption peak drops through the probe frequency depends on the strength of the excitation: the higher the pump fluence, the faster Re($\varepsilon$) drops through zero. Figure 5 illustrates this dependence by showing the time delay at which Re($\varepsilon$) crosses through zero plotted vs. pump fluence. For fluences around 2.0 $kJ/m^2$, the absorption peak comes into resonance with the probe frequency within a few hundred femtoseconds; at fluences just above 0.8 $kJ/m^2$, on the other hand, the absorption peak takes on the order of 10 picoseconds to come into resonance. For fluences below 0.8 $kJ/m^2$, Re($\varepsilon$) never goes through zero, indicating that the excitation is not strong enough to bring the resonant frequency of the peak down to the probe frequency.

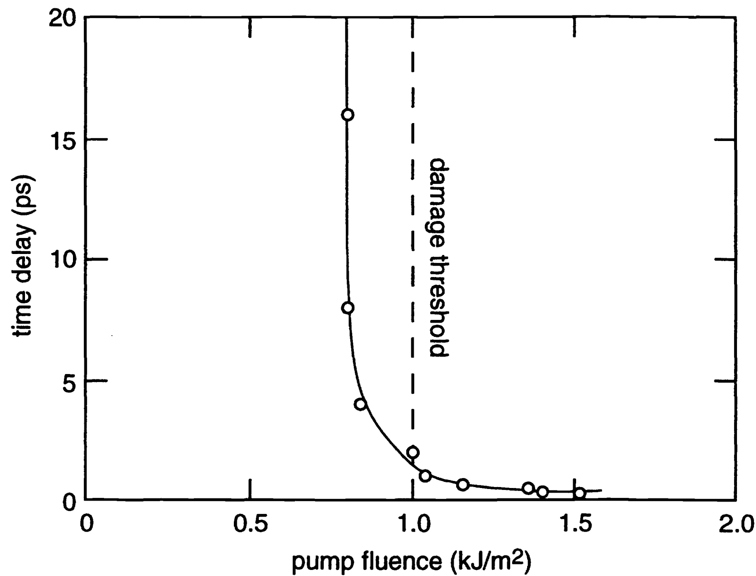


**Figure 5.** Pump-probe time delays at which Re($\varepsilon$) = 0 for different pump fluences. The solid curve is drawn to guide the eye, and the dashed line corresponds to the damage threshold of 1.0 kJ/m$^2$. At fluences above this value, the induced changes in the material are irreversible, while at fluences below the damage threshold the induced changes are reversible.

The dashed line in Fig. 5 at 1.0 kJ/m$^2$ indicates the threshold fluence for permanent damage to the sample. We determined this threshold by correlating pump pulse fluence with the size of damage spots on the sample measured through a microscope. Above the damage threshold the pump pulse induces irreversible changes in the sample while below the damage threshold the induced changes are reversible. Measurements taken several seconds after the excitation confirm that the dielectric constant eventually returns to its initial value for fluences below the damage threshold. Note, however, that the absorption peak comes into resonance with the probe frequency even for pump fluences below this damage threshold.

Qualitatively, we can approximate the dielectric function of GaAs by a damped single harmonic oscillator with a resonant frequency equal to the average bonding-antibonding splitting,[16] which in the ground state is about 4.75 eV.[17,25] If we associate the absorption peak in the data with the harmonic oscillator peak corresponding to the bonding-antibonding splitting, then the observed sweeping of the absorption peak frequency through the probe laser frequency implies a drop in average bonding-antibonding splitting from 4.75 eV to below 2.2 eV. Note that this drop in the average splitting by more than a factor of two occurs even for fluences below the damage threshold, when the induced changes are reversible.

The laser-induced drop in the bonding-antibonding splitting is schematically illustrated in Figure 6. The average bonding-antibonding splitting $\omega_0$ starts out far above 2.2 eV, so the probe photon energy lies at the foot of the single-oscillator absorption peak where Im($\varepsilon$) is small (step 1 in Fig. 6). After excitation, $\omega_0$ begins to decrease, leading to a downward shift in the resonant frequency of the single-oscillator absorption peak and therefore a rise in Im($\varepsilon$) at 2.2 eV (step 2 in Fig. 6). As $\omega_0$ drops past 2.2 eV (step 3 in Fig. 6), Im($\varepsilon$) goes through a peak. If $\omega_0$ drops far enough, the minimum in the conduction band will drop below the maximum in the valence band and the semiconductor will take on metallic properties (step 4 in Fig. 6).

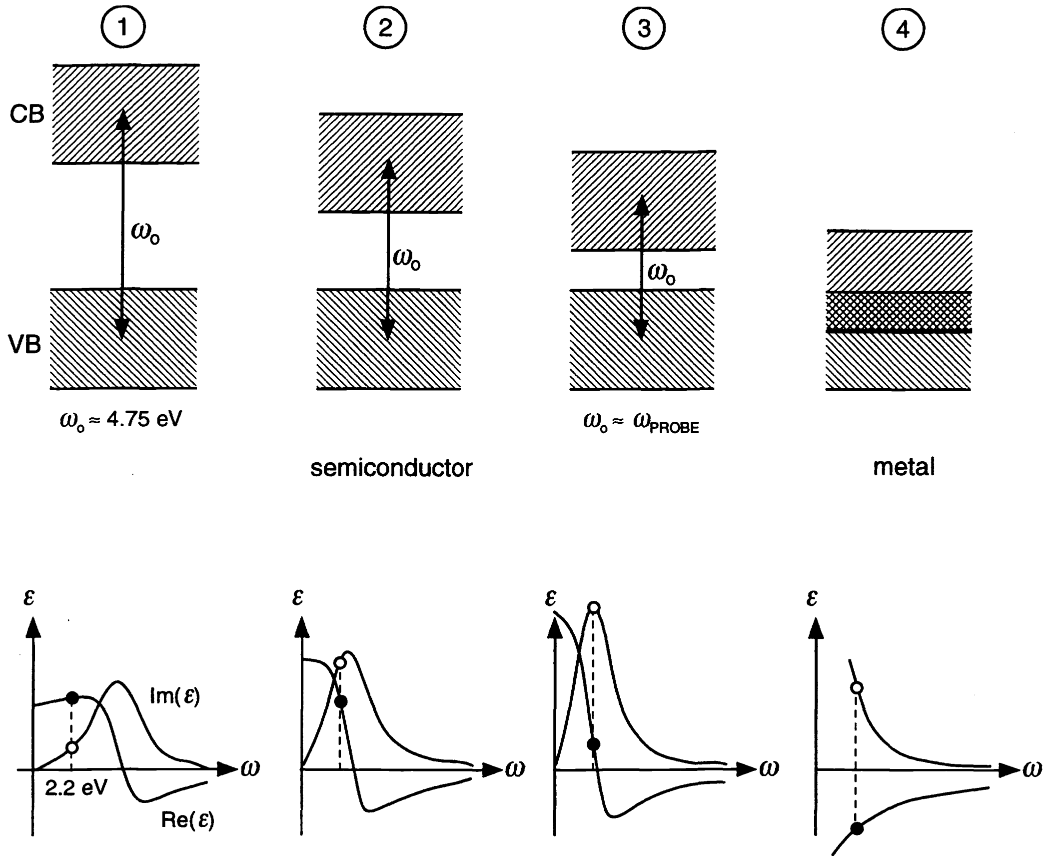


**Figure 6.** Schematic representation of the bandgap collapse. The pump pulse leads to a drop in the average bonding-antibonding splitting from its initial value of about 4.75 eV to below the probe photon energy of 2.2 eV. The drop in average bonding-antibonding splitting appears as a shift in the main absorption peak in the dielectric function, as illustrated at the bottom.

## 3. DIRECT MEASUREMENT OF THE DIELECTRIC CONSTANT AT 4.4 eV

This interpretation of the 2.2-eV data in terms of a drop in the average bonding-antibonding splitting allows us to predict qualitatively the behavior of the dielectric constant at different photon energies under similar excitation conditions. In particular, for a given excitation strength, the dielectric constant at a probe photon energy between 2.2 eV and 4.75 eV should exhibit resonance features at an earlier pump-probe time delay than the dielectric constant at 2.2 eV. Equivalently, for a fixed pump-probe time delay, the dielectric constant at a probe photon energy in the above range should exhibit resonance features at a lower pump fluence than the dielectric constant at 2.2 eV.

We verified this prediction by measuring the behavior of the dielectric constant using frequency-doubled probes at 4.4 eV, just below the initial value of the average bonding-antibonding splitting of GaAs. Figure 7 shows time-dependence of the 4.4-eV dielectric constant at the same four pump fluences shown in Fig. 3. Note that Im($\varepsilon$) now starts near the peak and that the zero-crossings in Re($\varepsilon$) occur at lower fluences than at 2.2 eV. This can also be seen in Fig. 8, which adds to Fig. 4 the corresponding points for the 4.4-eV data. At 4.4 eV, Re($\varepsilon$) crosses zero for fluences as low as 0.5 kJ/m$^2$, well below the 0.8 kJ/m$^2$ required at 2.2 eV.

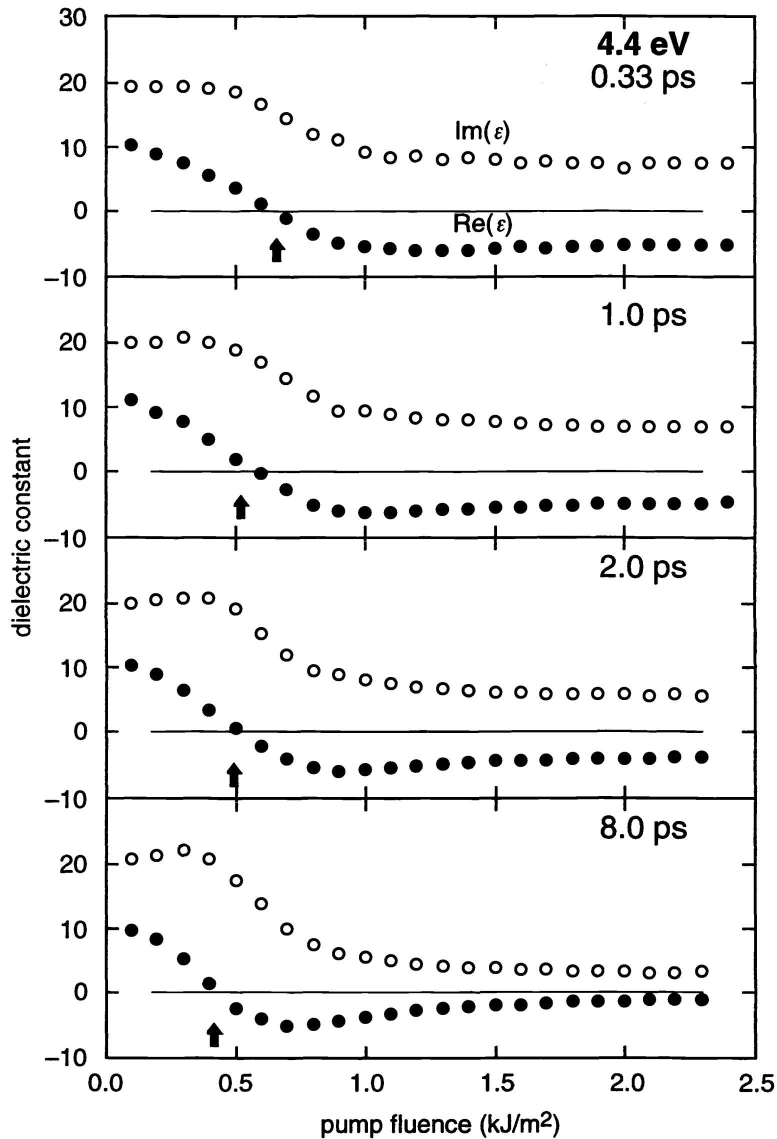


**Figure 7.** Dielectric constant at 4.4 eV vs. pump fluence for four different pump-probe time delays. ●: Re(ε), ○: Im (ε).

The behavior of the dielectric constant at 4.4 eV is indeed consistent with the proposed picture of a drop in the average bonding-antibonding splitting. Following the pump pulse excitation, $\omega_0$ drops from its initial value of about 4.75 eV first past 4.4-eV and then continues down past 2.2-eV. A stronger excitation causes a faster drop through both probe frequencies. At pump fluences between 0.5 kJ/m$^2$ and 0.8 kJ/m$^2$, the excitation is strong enough to bring the resonant frequency of the absorption peak below 4.4 eV but not all the way down to 2.2 eV. Note that since 4.4 eV is close to the initial value of the average bonding-antibonding splitting, Im[e(4.4 eV)] does not rise much above its initial value before coming down.

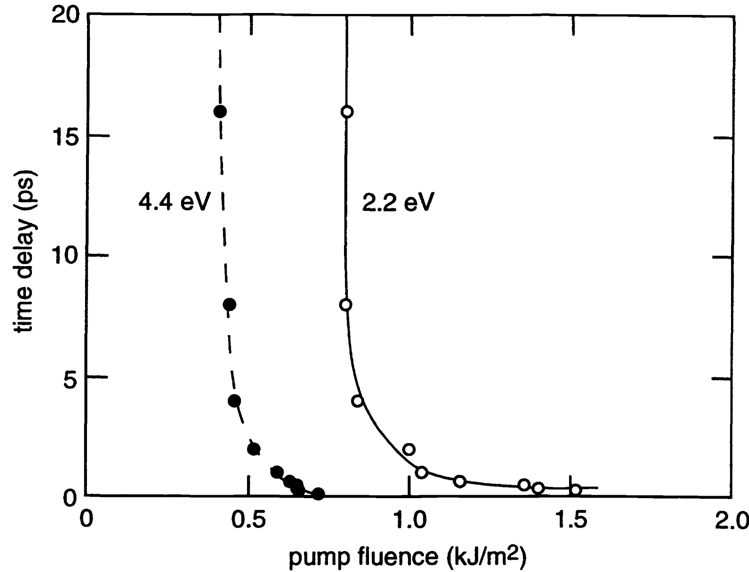


**Figure 8.** Pump-probe time delays at which Re(e) = 0 for different pump fluences at both 2.2 eV and 4.4 eV. The curves are drawn to guide the eye. l: 4.4 eV, l: 2.2 eV.

## 4. BROADBAND MEASUREMENTS

We have recently moved beyond single-frequency measurements using a new broadband spectroscopic technique to simultaneously monitor the response of the dielectric function $\varepsilon(\omega)$ of GaAs across the spectral range from 1.5 to 3.5 eV, with 100-fs temporal resolution.

The GaAs sample is driven by a 1.9-eV pump pulse and probed by a broadband probe pulse generated by strong self-phase modulation of a 70-fs 2.2-eV pulse in $CaF_2$. Reflectivities $R_1(\omega)$ and $R_2(\omega)$ are measured for p-polarized light at two incident angles, 58° and 75°, chosen to give high sensitivity to changes in the dielectric function. The reflectivity is determined by measuring with an imaging spectrometer both the reflected probe spectrum and a reference spectrum for each shot. The real and imaginary parts of the dielectric function are then evaluated using an optimization algorithm which finds the $\varepsilon(\omega)$ which gives the experimental reflectivities using the Fresnel equations and a three-layer model which takes account of an oxide layer of thickness 3.5 nm and $\varepsilon = 4$ on the bulk GaAs sample. By varying the time delay between the pump and the probe, we observe the changes in the dielectric function in time as a result of the intense excitation. The broadband probe has significant temporal dispersion for which we compensate by temporally shifting the data based on a measured calibration of the dispersion.

The data in Fig. 9 show $\varepsilon(\omega)$ at 500 fs and 4 ps after excitation by a pulse of 45% of the threshold for observable permanent change. Also shown in Fig. 9*a* are the real and imaginary parts of the unperturbed $\varepsilon(\omega)$ (solid and dashed curves). The 500-fs data display a drop in the real part and a broadening in the imaginary part of the dielectric function directly following the excitation. By 4 ps $\varepsilon(\omega)$ has changed considerably and agrees closely with ellipsometric measurements on GaAs at elevated temperature,[26] shown at 770 K by the solid and dashed curves in Fig. 9*b*. While the initial effects are likely electronic in this fluence regime, by 4 ps the lattice has been heated by the electrons and this process dominates the changes in $\varepsilon(\omega)$.

At a higher fluence of 70% of the threshold, the changes in $\varepsilon(\omega)$ are much more pronounced, as shown in Fig. 10 at 500 fs and 4 ps. At 500 fs, the imaginary part of $\varepsilon(\omega)$ is very broadly spread across the entire spectral range, and the real part has decreased. By 4 ps, the dielectric function is quite similar to that of amorphous

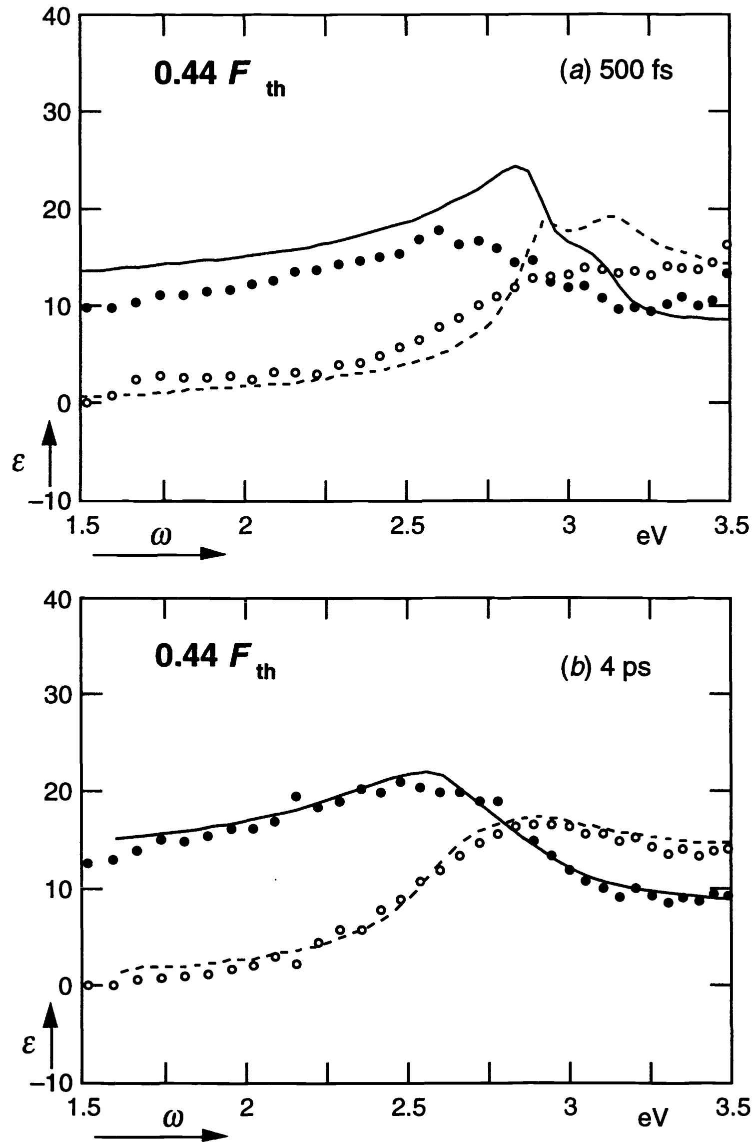


**Figure 9.** Dielectric function of GaAs at a pump fluence of 0.45 kJ/m$^2$ after (*a*) 500 fs and (*b*) 4 ps; •: Re[$\varepsilon(\omega)$], o: Im[$\varepsilon(\omega)$]. The curves in (*a*) represent the real (solid curve) and imaginary (dashed curve) parts of the dielectric function for unpumped GaAs at 300 K. The curves in (*b*) show the dielectric function of GaAs at 770 K.[26]

GaAs[27] (see curves), suggesting that the material has become disordered. It is interesting to note that this disordering occurs below the threshold for permanent change and thus the changes must be reversible.

Above the damage threshold $\varepsilon(\omega)$ changes dramatically. Figure 11 shows $\varepsilon(\omega)$ at 500 fs and 4 ps after an excitation of 160% of the threshold. Within 500 fs, much of the oscillator strength has moved from the large $E_2$ peak (initially centered at 4.75 eV) down to the probed spectral range. The real part is negative above 2.7 eV because most of the oscillator strength is at lower frequencies. By 4 ps the real part is negative above 1.8 eV, and possibly even below 1.8 eV. The metal-like dielectric function above 1.8 eV can be fitted with a Drude model, which gives a 12-eV plasma frequency and a 0.2-fs relaxation time. The large plasma frequency indicates

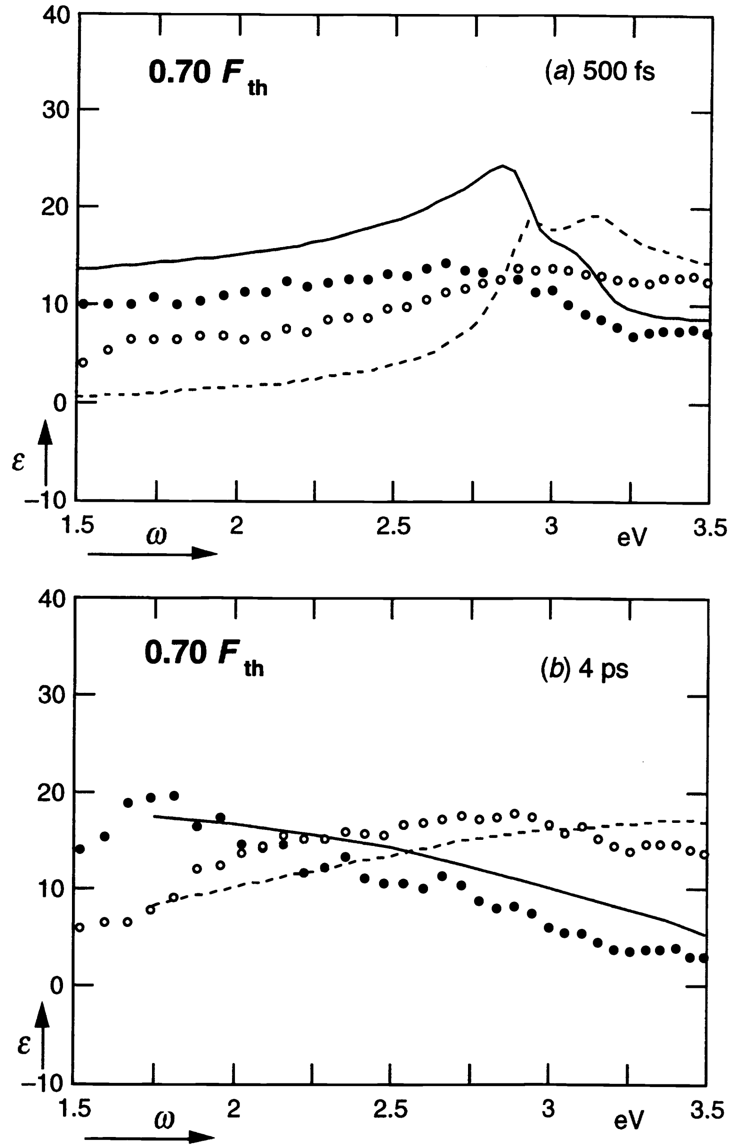


**Figure 10.** Dielectric function of GaAs at a pump fluence of 0.75 kJ/m$^2$ after (*a*) 500 fs and (*b*) 4 ps; •: Re[$\varepsilon(\omega)$], o: Im[$\varepsilon(\omega)$]. The curves in (*a*) represent the real (solid curve) and imaginary (dashed curve) parts of the dielectric function for unpumped GaAs. The curves in (*b*) show the dielectric function of amorphous GaAs [27]

that almost all of the original valence electrons are behaving as free carriers. The changes in the dielectric function are much more drastic than those due to disordering and indicate changes in local bonding.

## 5. DISCUSSION

What underlying physical effects are responsible for the alteration of the band structure illustrated by the changes in the dielectric function? To answer this question, we should examine two main sources of band-

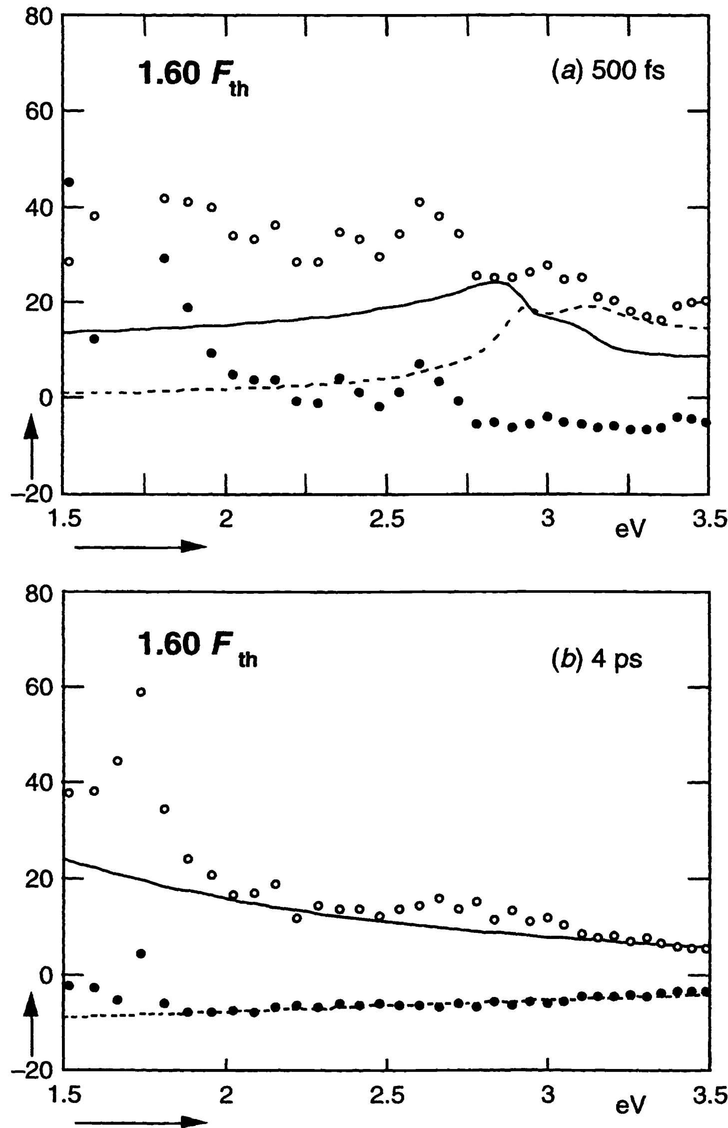


**Figure 11.** Dielectric function of GaAs at a pump fluence of 1.6 kJ/m$^2$ after (*a*) 500 fs and (*b*) 4 ps; •: Re[$\varepsilon(\omega)$], o: Im[$\varepsilon(\omega)$]. The curves in (*a*) represent the real (solid curve) and imaginary (dashed curve) parts of the dielectric function for unpumped GaAs. The curves in (*b*) represent a fit of the data to a Drude model.

structure modification: electronic screening and structural change. Through electron-hole pair generation, the pump pulse creates a large population of mobile charge carriers that can partially screen the ionic potential in the material. Because the average bonding-antibonding splitting increases with the strength of the ionic potential,[25] electronic screening reduces the average bonding-antibonding splitting. A recent calculation shows that when 10% of the valence electrons are excited to the conduction band, the direct gap at the X-point in the band structure of GaAs will decrease by roughly 2 eV due to electronic screening and many-body bandgap renormalization while the direct gap at the Γ-point changes only slightly.[18]

Because the strength of electronic screening increases with the free-carrier density, the effects due to screening should follow the carrier density instantaneously. Therefore, the effect of screening on the dielectric constant should be largest when the free carrier density is highest—*i.e.* immediately following the excitation. As Auger recombination and diffusion reduce the free-carrier density, the influence of electronic screening on the band structure should correspondingly decrease. However, as can be seen in Fig. 2, the changes in dielectric constant continue to grow for picoseconds following excitation, when the carrier density is already decreasing from its peak value. Clearly, electronic screening cannot, by itself, account for the observed behavior.

Since the band structure is determined by the crystal structure, changes in the atomic arrangement can also account for the observed collapse of the bandgap. Deformation of the diamond or zincblende structure in a semiconductor is known to lead to a collapse of the band gap and a semiconductor-metal transition.[19-21,25] Just a 10% change in average bond length is enough to cause a semiconductor-metal transition[21]. Note that an ionic velocity as small as 25 m/s is already sufficient to achieve a 10% change in the GaAs bond length within 1 ps.

In semiconductors like GaAs the covalent bonds are stabilized by the valence electrons, so excitation of a large number of electrons from bonding valence states to antibonding conduction states can lead directly to lattice instability[5,22,23]. If the femtosecond laser pulse is intense enough to excite this critical density of electrons, the resulting instability causes the lattice to deform — a deformation which begins immediately following the excitation but continues long after the incidence of the pump pulse. The change in the dielectric constant accompanying the lattice deformation should therefore continue to increase in the picoseconds following the excitation, in agreement with the observed behavior of the dielectric constant.

## ACKNOWLEDGMENTS

We wish to thank Profs. N. Bloembergen, E. Kaxiras, and H. Ehrenreich for many valuable comments. This work is supported by the Joint Services Electronics Prograrm under contract number ONR N00014-89-J-1023..

## REFERENCES

1. E.I. Shtyrkov, I.B. Khaibullin, M.M. Zaripov, M.F. Galyatudinov, R.M. Bayazitov, *Sov. Phys-Semicond.*, **9**, 1309 (1976).
2. R.F. Wood, C.W. White, R.T. Young, Eds. *Semiconductors and Semimetals*, Vol. **23** (Academic Press, New York, 1984).
3. A.M. Malvezzi, H. Kurz, N. Bloembergen, in *Energy Beam-Solid Interactions and Transient Thermal Processing*, Eds. D. K. Biegelsen, G.A. Rozgonyi and C.V. Shank (Materials Research Society, Pittsburgh, 1985).
4. A.M. Malvezzi, in *Excited-State Spectroscopy in Solids*, Eds. U.M. Grassano, N. Terzi (North-Holland, Amsterdam, 1987).
5. J.A. Van Vechten, R. Tsu, and F.W. Saris, *Phys. Lett.* **74A**, 422 (1979).
6. J.A.. Van Vechten, in *Semiconductors Probed by Ultrafast Laser Spectroscopy*, Ed. R.R. Alfano (Academic Press, San Diego, 1984).
7. D.K. Biegelsen, G.A. Rozgonyi, C.V. Shank, Eds., *Energy Beam-Solid Interactions and Transient Thermal Processing*, Vol. **35** (Materials Research Society, Pittsburgh, 1985).
8. C. V. Shank, R. Yen, and C. Hirlimann, *Phys. Rev. Lett.* **51**, 900 (1983)..
9. M.C. Downer, R.L. Fork, and C.V. Shank, J. Opt. Soc. Am. B **2**, 595 (1985).
10. H.W.K. Tom, G.D. Aumiller, and C.H. Brito-Cruz, *Phys. Rev. Lett.* **60**, 1438 (1988).
11. S.V. Govorkov, I.L. Shumay, W. Rudolph, and T. Schroeder, *Opt. Lett.* **16**, 1013 (1991).
12. K. Sokolowski-Tinten, H. Schulz, J. Bialkowski, and D. von der Linde, *Appl Phys A* **53**, 227 (1991).
13. P. N. Saeta, J. Wang, Y. Siegal, N. Bloembergen, and E. Mazur, *Phys. Rev. Lett.* **67**, 1023 (1991).

14. H. Kurz, and N. Bloembergen, in *Energy Beam-Solid Interactions and Transient Thermal Processing*, Eds. D.K. Biegelsen, G.A. Rozgonyi and C.V. Shank (Materials Research Society, Pittsburgh, 1985).
15. D.L. Greenaway, and G. Harbeke, *Optical Properties and Band Structure of Semiconductors*; (Pergamon Press, Oxford, 1968).
16. M.L. Cohen, and J.R. Chelikowsky, *Electronic Structure and Optical Properties of Semiconductors*; (Springer-Verlag, Berlin, 1988).
17. D.E. Aspnes, G.P. Schwartz, G.J. Gualtieri, A.A. Studna, and B. Schwartz, *J. Electrochem. Soc.* **128**, 590 (1981).
18. D.H. Kim, H. Ehrenreich, and E. Runge, *Solid State Commun.* **89**, 119 (1994).
19. V.M. Glazov, S.N. Chizhevskaya, and N.N. Glagoleva, *Liquid Semiconductors* (Plenum Press, New York, 1969).
20. W. Jank, and J. Hafner, *J. Non-Crystalline Solids* **114**, 16 (1989).
21. S. Froyen, and M. L. Cohen, *Phys. Rev. B* **28**, 3258 (1983).
22. R. Biswas, and V. Ambegoakar, *Phys. Rev. B* **26**, 1980 (1982).
23. P. Stampfli, and K.H. Bennemann, *Phys. Rev. B* **42**, 7163 (1990).
24. C.V. Shank, R. Yen, C. Hirlimann, *Phys. Rev. Lett.* **50**, 454 (1983).
25. W.A. Harrison, *Electronic Structure and the Properties of Solids: The Physics of the Chemical Bond* (Dover, New York, 1989).
26. H. Yao, P. G. Snyder, and J. A. Woollam, *J. Appl. Phys.* **57**, 3261 (1991).
27. M. Erman, J. B. Theeten, P. Chambon, S. M. Kelso and D. E. Aspens, *J. Appl. Phys.* **56**, 2664 (1984).
28. Y. Siegal, E.N. Glezer, E. Mazur, *Phys. Rev. B* **49**, 16403 (1994).
29. E.N. Glezer, Y. Siegal, L. Huang, E. Mazur, *Phys. Rev. B* **51**, 6959 (1995).